Transmission Characteristics of Long-Range Dielectric-Loaded Surface Plasmon Polariton Waveguide Based on Golden Ratio

Shao Xiaozhen Zhang Guanmao Wang Qiong Hu Nan

Institute of Modern Communication Technology, School of Information Science and Engineering, Lanzhou University, Lanzhou, Gansu 730000, *China*

Abstract A novel long-range dielectric-loaded surface plasmon polariton waveguide (LR-DLSPPW) structure based on the golden ratio is proposed. Transmission characteristics, like the normalized electric field distribution, mode effective index, attenuation constant, propagation distance, mode width, figure of merit (FOM), and coupling length of this kind of waveguide, have been analyzed and numerically calculated via the finite element method at the telecom wavelength of $\lambda_0 = 1.55$ μm. The results show that the LR-DLSPPW based on the golden ratio has a longer propagation distance of 1.36 mm and a smaller mode width of 1.35 μm compared to non-golden ratio waveguides. When the height-width ratio of the dielectric ridge is at the golden ratio with a fixed area of 0.9 μm^2, its FOM has a maximum value larger than 6.15×10^5. In addition, the crosstalk can be ignored when the distance between two adjacent waveguides exceeds 3 μm. Consequently, the designed waveguide has significant potential for applications in design of high density integrated optoelectronic circuits.

Key words integrated optics; surface plasmon polariton waveguides; finite element method; golden ratio; transmission characteristics

OCIS codes 130.3120; 130.2790; 240.6680

基于黄金分割比的长程介质加载表面等离子激元波导传输特性研究

邵晓珍 张冠茂 王 琼 胡 南

兰州大学信息科学与工程学院现代通信技术研究所，甘肃 兰州 730000

摘要 提出了一种基于黄金分割比的新型长程介质加载表面等离子激元波导(LR-DLSPPW)结构，在通信波长 $\lambda_0=1.55$ μm 情形下，运用有限元法对这种波导基模的归一化电场分布、模式有效折射率、衰减常数、传播长度、模式宽度、品质因数和耦合长度等传输特性参数进行了仿真分析计算。结果表明，与不具有黄金分割比的类似波导相比，基于黄金分割比的 LR-DLSPPW 具有较长的传播长度 1.36 mm 和较小的模式宽度 1.35 μm；另一方面，当介质脊面积保持为 0.9 μm^2 不变且介质脊高宽比值取为黄金分割比时，其品质因数会出现一个超过 6.15×10^5 的最大值。此外，当相邻波导之间的间隔超过 3 μm 时，相邻波导间的串扰可被忽略。显然，这种基于黄金分割比的新型波导结构能够很好地应用于高密度光子集成回路的设计中。

关键词 集成光学；表面等离子激元波导；有限元法；黄金分割比；传输特性

中图分类号 O436 **文献标识码** A

doi: 10.3788/LOP53.061301

收稿日期：2015-10-26；**收到修改稿日期**：2016-01-11；**网络出版日期**：2016-05-25

基金项目：中央高校基本科研业务费专项资金(lzujbky-2012-40，lzujbky-2015-K7)

作者简介：邵晓珍 (1990－)，女，硕士研究生，主要从事表面等离子激元波导技术应用方面的研究。E-mail：13658348125@163.com

导师简介：张冠茂 (1973－)，男，博士，副教授，硕士生导师，主要从事光通信、光传感、微纳光子晶体以及光域表面等离子激元共振理论与应用等方面的研究。E-mail：zhanggm@lzu.edu.cn(通信联系人)

1 Introduction

Over the past decade or so, plasmonic polariton waveguides have gained extensive attention due to their ability to confine electromagnetic modes on the sub-wavelength scale. Hence, they provide the possibility to fabricate high density integrated photonic circuits[1]. Surface plasmon polaritons (SPPs) are electromagnetic waves (EMs) propagating at the interface between a dielectric and a metal conductor that can confine the EMs at the sub-wavelength scale beyond the diffraction limit[2-4]. The electromagnetic fields of SPPs reveal a maximum value at the metal-dielectric interface that decays exponentially away from it, thus exhibiting a strong intrinsic confinement in the direction perpendicular to the interface[2]. Because of the SPP field confinement properties, a great variety of plasmonic waveguides based on SPPs have been investigated and validated over the past several years. These plasmonic waveguides include metallic stripes[5], metallic nanowires[6], channel SPP waveguides[7], dielectric-loaded SPP waveguides (DLSPPWs) which place a thin dielectric ridge on the surface of the metal[8-11], long-range dielectric-loaded SPP waveguides (LR-DLSPPWs) which insert a thin metallic stripe into the dielectric ridge[12-13] and so on. Several plasmonic devices have been designed and manufactured based on these waveguides[14-17]. However, for these waveguides, there is a common obstacle, i.e. the trade-off between the propagation distance and the field confinement. For example, DLSPPWs have a better field confinement, but the propagation distance is relatively short[9,18]. In order to overcome this problem, LR-DLSPPWs have been investigated[10,19-20], which can not only ensure considerable propagation distance, but also have a wavelength scale mode confinement. Therefore, they can better balance between the sub-wavelength constraint and the transmission loss related to the metal. Furthermore, this type of waveguide provides an additional opportunity to control plasmonic signals by modifying the properties of the dielectric forming the guide[21-22]. Currently, LR-DLSPPWs are made of low index dielectric polymers[23]. Lately, in order to integrate the photon loop into the electronic chip, the DLSPPW technology is introduced into the CMOS logic circuit. The high refractive index of the materials used to manufacture the DLSPPWs should be matched with the manufacturing process of the electric chip. Hence, silicon, as a high refractive index material, has been mainly used[24]. Recently, the LR-DLSPPW technology has been applied to the design of the CMOS logic circuit, thus an LR-DLSPPW with a high refractive index that can be matched with the CMOS logic circuit has been proposed and investigated[25].

In order to further optimize the trade-off between the propagation distance and the mode width of the LR-DLSPPW that can be matched with the CMOS logic circuit, a novel LR-DLSPPW structure based on the golden ratio is proposed. The research on the fundamental mode transmission characteristics of the waveguide is carried out at the telecom wavelength of $\lambda_0 = 1.55$ μm, and the characteristics include the normalized electric field distribution of the fundamental mode, mode effective index, propagation distance, mode width, figure of merit (FOM), and coupling length[26]. When compared with traditional LR-DLSPPWs that can be matched with the CMOS logic circuit, this waveguide does a better confine the field in the dielectric ridge, but also has a longer propagation distance and higher FOM. Therefore, this kind of waveguide can offer a higher value for practical applications to fabricate plasmonic devices. All simulations are performed by using rigorous numerical schemes based on the finite element method (FEM). The basic idea of the FEM is to divide the computational domain into many finite triangle areas through the weighted residual quantity method and variation principle. In the process of solving, we selecte some nodes in each grid as interpolation points, and then rewrite the variables of the differential equations into linear expressions that are composed of the interpolation functions and the variables′ derivatives. Finally, we solve the differential equations using the weighted residual quantity method and variation principle. For the designed waveguide in this paper, we selected, for boundary conditions, a perfect magnetic conductor field around the outside and inside is continuous. At the same time, we set up the communication wavelength at $\lambda_0 = 1.55$ μm, and the field type and solving methods are the hybrid-mode wave and mode analysis, respectively.

2 Theoretical analysis and waveguide structures

The diagram of the LR-DLSPPW based on the golden ratio is shown in Fig. 1. The waveguide is composed of a thin copper film (with thickness h, width g, and refractive index n_2) embedded in a golden rectangle ridge (with thickness t, width w, area S_0, and refractive index n_1) which is composed of silicon nitride (Si_3N_4) surrounded by air (with refractive index n_0), and two semiconducting dielectric layers (SiO_2 and Si) which are supported by a 2-μm-thick SiO_2 layer (with refractive index n_3) and a silicon substrate (with refractive index n_4). Furthermore, the formed top of SiO_2 is used to thermally oxidize the Si layer. The thickness of the Si layer decreases with

increasing thickness of the layer, but there is a relative ratio between them, i.e. 1 (silicon) to 2.27 (SiO_2)[27]. If we set the initial and final thicknesses of the silicon layer to be t_0 and t_1, respectively, the thickness of the upper SiO_2 layer can be solved by the formula $t_2=(t_0-t_1)\times 2.27$. In addition, several fundamental parameters are used in the numerical calculation of this waveguide as follows. For the golden rectangle dielectric ridge, $n_1=1.98$[27]; for the copper film, $n_2=0.606+8.92$i, $g=500$ nm, $h=15$ nm[27]; for the SiO_2 layer, $n_3=1.45$[27]; and for the Si layer, $n_4=3.48$[27]. COMSOL Multiphysics, a simulation software, is used to perform numerical simulations and the telecom wavelength is selected as $\lambda_0=1.55$ μm in the process.

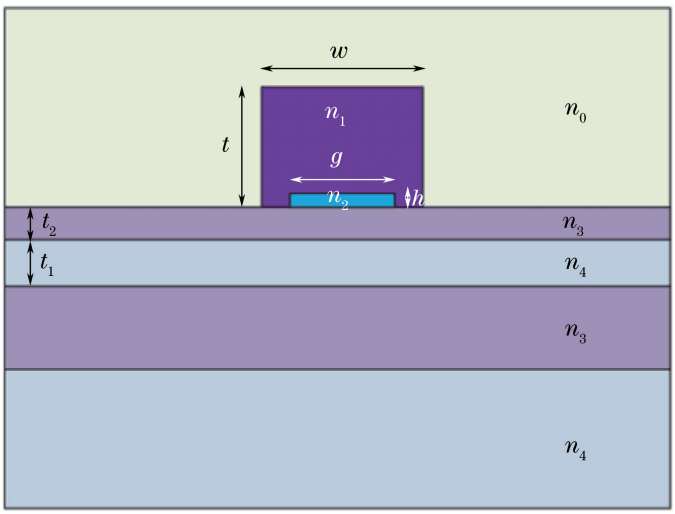

Fig. 1 Diagram of the cross section of the LR-DLSPPW based on the golden ratio

In SPP waveguides, the propagation distance can be calculated by the following formula:

$$L_P=\frac{\lambda_0}{4\pi \mathrm{Im}(n_{\mathrm{eff}})}, \tag{1}$$

where $\mathrm{Im}(n_{\mathrm{eff}})$ is the imaginary part of the effective mode index n_{eff}. Better mode field confinement can ensure smaller mode width, and smaller mode width is good for high density integration components in the integrated circuit, which furthermore reduces the transmission loss of unit elements. The mode width is the width of the peak at a field value of $1/e$[28]. The calculation of the mode width is used to classify the field column m, and each column gets n electric field values. Then we add the absolute value of the electric field of each column, and use array $\boldsymbol{A}$ ($\boldsymbol{A}=[a_1,a_2,\cdots,a_m]$) to express the obtained m data. Secondly, we find the maximum value of array $\boldsymbol{A}$, expressed by $\max(a_1,a_2,\cdots,a_m)$; then the data in the original array $\boldsymbol{A}$ is divided by $\max(a_1,a_2,\cdots,a_m)$. Array $\boldsymbol{B}$ ($\boldsymbol{B}=[b_1,b_2,\cdots,b_m]$) is used to express the obtained normalized m data. If there are b_p and b_q with a value in the vicinity of $1/e\approx 0.6379$ in array $\boldsymbol{B}$, and their transverse coordinates are x_1 and x_2, respectively, the mode width w can be written as follows:

$$w=|x_1-x_2|. \tag{2}$$

The FOM of the waveguide can be defined by the following formula[29]:

$$f_{\mathrm{FOM}}=L_p^2\frac{\lambda_0}{\mathrm{Re}(n_{\mathrm{eff}})\,w^3}, \tag{3}$$

where $\mathrm{Re}(n_{\mathrm{eff}})$ is the real part of the effective mode index n_{eff}.

3 Simulation results and discussion of transmission characteristics

3.1 Normalized electric field distribution of fundamental mode of waveguides

In order to investigate the transmission characteristics of the LR-DLSPPWs based on the golden ratio, we conducted the numerical simulation using the FEM. The normalized electric field (normalized with respect to the maximum value of the input electric field) distribution of the fundamental mode of the waveguide is shown in Fig. 2. The field is better confined in the rectangle ridge, the transmission loss in the waveguide is reduced, and the propagation distance is improved.

3.2 Influence of dielectric ridge area on mode effective index and attenuation constant

Firstly, in order to investigate some of the basic performance of the proposed novel waveguide, we carried out

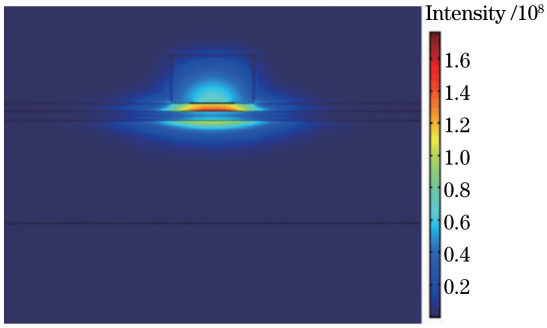

Fig. 2 Normalized electric field distribution of the fundamental mode of the designed waveguide

numerical simulations for this structure using the FEM method. The curves of the mode effective index and the attenuation constant versus the dielectric ridge area are given in Fig. 3. It can be observed that the total dielectric ridge area varies from 0.6 μm^2 to 1.4 μm^2. It can be discovered that the mode effective index increases with increasing dielectric ridge area, and the smaller the height-width ratio of the dielectric ridge is, the larger the mode effective index is when the area of the dielectric ridge is fixed. This is because the mode effective index is related to the dielectric on the surface of the metal. When the height-width ratio of the dielectric ridge decreases, the corresponding dielectric ridge width also decreases, which causes the weak confinement of the field.

In addition, we also find that the attenuation constant first decreases and then increases with the area increase of the dielectric ridge. Hence, for each of the curves of the height-width ratio, there is a minimum value, and for each of the curves, the corresponding area is different for every minimum value point. Moreover, the field attenuation is the smallest in the area distribution.

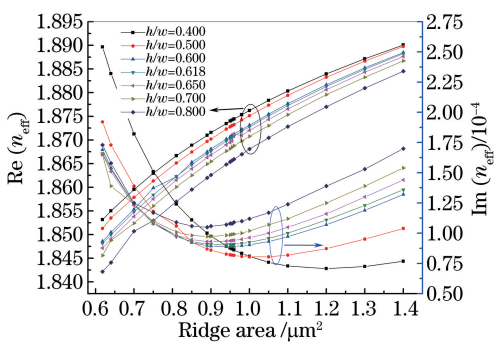

Fig. 3 Curves of the mode effective index and the attenuation constant versus the area distribution of the dielectric ridge

3.3 Influence of dielectric ridge area on propagation distance, mode width, and FOM

According to Fig. 3, we can calculate the propagation distance, mode width, and FOM of the waveguide at the telecom wavelength of $\lambda_0 = 1.55$ μm, and these curves versus the area distribution of the dielectric ridge are shown in Fig. 4.

Fig. 4(a) is the curve for the propagation distance. From the curves, we can see that, when other parameters are kept constant, the propagation distance initially increases with the increase of the area of the dielectric ridge, but when the dielectric ridge area reaches a certain threshold, the propagation distance rapidly decreases and for each of the curves, the dielectric ridge area corresponding to the maximum point of the propagation distance is different. The dielectric ridge area threshold shifts right along with the decrease of the height-width ratio. This is because of the loss of the plasmonic waves in the propagation, which is related to metal absorption loss. The larger the height-width ratio of the dielectric ridge is, the faster the attenuation increases. The larger attenuation constant corresponds to a smaller propagation distance, which is consistent of the attenuation constant curve in Fig. 3.

Fig. 4(b) is the curve of the mode width versus the dielectric ridge area. We can observe that the mode width increases with the increase of the dielectric ridge area for each of the curves of the height-width ratio of the dielectric ridge, and for a fixed dielectric ridge area, the smaller the height-width ratio of the dielectric ridge is, the larger the mode width is. This is because of the increase of the dielectric ridge width. The dielectric ridge for the field is weakly confined when the dielectric ridge area constant is kept constant and the height-width ratio of the dielectric

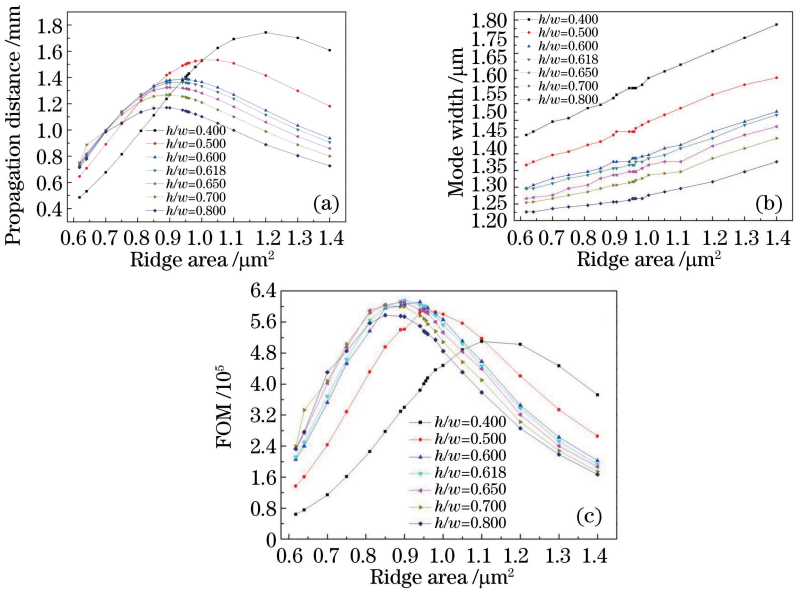

Fig. 4 Variation relationship between area distribution of the dielectric ridge and (a) propagation distance; (b) mode width; (c) FOM

ridge is smaller.

Fig. 4(c) is the curve of FOM versus dielectric ridge area. We can see from the figure that the tendency for FOM is initially increasing and then decreasing as the dielectric ridge area continues to increase. When the ridge area is 9.0 μm^2, the height-width ratio of the dielectric ridge is 0.618. This dielectric ridge is a golden rectangle, and the maximum value of FOM exceeds 6.15×10^5. Therefore, for further study of the transmission performance of the fundamental mode of the proposed waveguide, all simulations are based on the golden rectangle in which the dielectric ridge area is 9.0 μm^2.

3.4 Influence of height-width ratio of dielectric ridge on mode effective index and attenuation constant

We investigated the influence of the height-width ratio of the dielectric ridge on the mode effective index and the attenuation constant when other parameters were kept constant. The relevant calculation results are shown in Fig. 5. We can observe from the curves that the mode effective index increases initially, then decreases with increasing height-width ratio of the dielectric ridge, and reaches a maximum value when the height-width ratio of the dielectric ridge is about 0.35. Additionally, the attenuation constant initially decreases and then increases with increasing height-width ratio of the dielectric ridge, and a minimum value is obtained when the height-width ratio of the dielectric ridge is about 0.5. At this point, the field attenuates slowly, which is one of the advantages in the wave transmission.

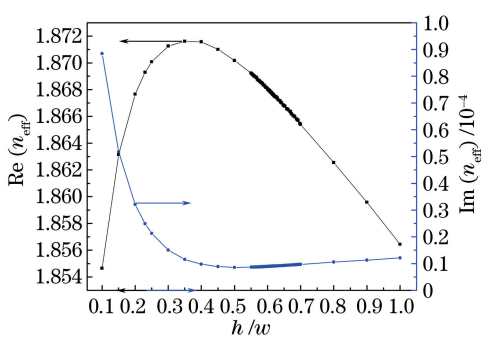

Fig. 5 Curves of the mode effective index and the attenuation constant versus the height-width ratio of the dielectric ridge

3.5 Influence of height-width ratio of dielectric ridge on propagation distance, mode width, and FOM

In order to further investigate the characteristics of the waveguide with respect to the height-width ratio of the dielectric ridge, the relationships between propagation distance, mode width, FOM of the waveguide and the height-width ratio of the dielectric ridge are calculated and shown in Fig. 6.

Fig. 6(a) shows the curves of the propagation distance versus the height-width ratio of the dielectric ridge. We

can see from the curves that the propagation distance increases initially and then decreases with increasing height-width ratio of the dielectric ridge, and reaches a maximum value when the height-width ratio of the dielectric ridge is about 0.5, corresponding to the attenuation constant which has a minimum value at this point. According to the definition of the propagation distance, the lower the attenuation is, the longer the transmission is.

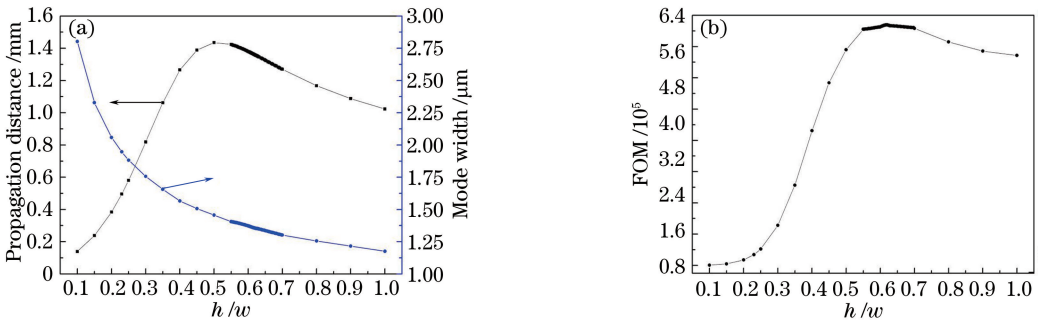

Fig. 6 Relationship between (a) propagation distance, mode width, (b) FOM and the height-width ratio of the dielectric ridge

The curves of the mode width versus the height-width ratio of the dielectric ridge are shown in Fig. 6(a). We find that the mode width decreases with increasing height-width ratio of the dielectric ridge. This is because the width of the dielectric ridge decreases with increasing height-width ratio of the dielectric ridge when the dielectric ridge area is kept constant, which causes the weakly confined field.

In addition, Fig. 6(b) shows the curve of FOM versus the height-width ratio of the dielectric ridge. It is observed that FOM initially increases and then decreases with increasing height-width ratio of the dielectric ridge, and the maximum value is obtained when the height-width ratio of the dielectric ridge is about 0.618. Taking into consideration that FOM is a key factor to estimate the overall performance of the waveguides, when it obtains its largest value, as illustrated in the proportion relationship, this waveguide has optimal comprehensive performance. This point is a very useful reference value for designing and processing plasmonic waveguides and optoelectronic devices.

3.6 Relationship among many parameters to evaluate waveguide performance

We can see from Fig. 7(a) that the propagation distance decreases with increasing normalized attenuation constant. This is consistent with the theory of SPP wave propagation, i.e. the smaller the attenuation is, the longer the propagation is. From Fig. 7(b), we can observe that FOM and the propagation distance first increase and then decrease with the increase of the mode width, and FOM decreases faster than the propagation distance.

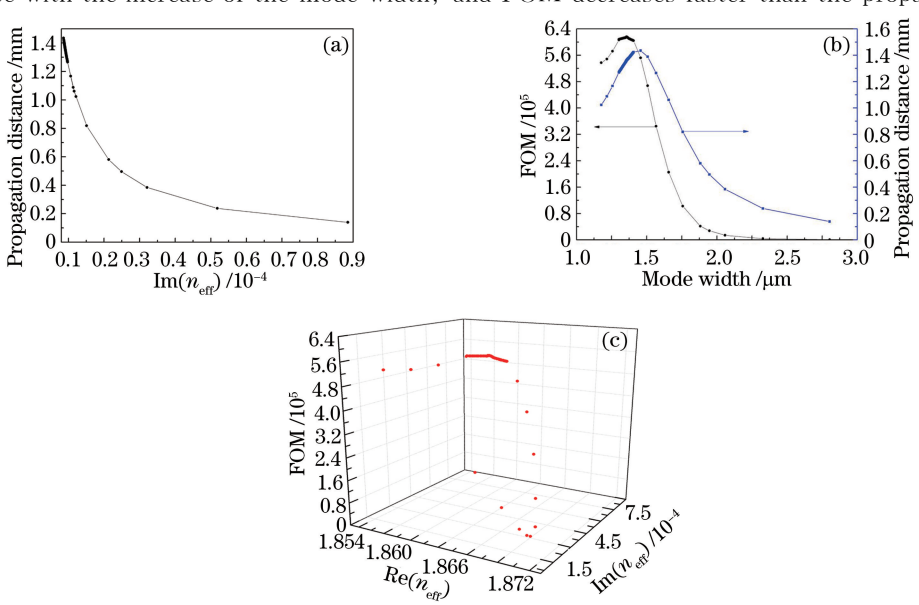

Fig. 7 Curves of (a) propagation distance versus the attenuation constant; (b) FOM and propagation distance versus mode width; (c) three-dimensional scatter map of FOM versus mode effective refractive index and normalized attenuation constant

This is because FOM is proportional to the square of the propagation distance, and is inversely proportional to the cube of the mode width from the computational formula for FOM. Additionally, from Fig. 7(c), we draw the three-dimensional scatter map of FOM versus the mode effective refractive index and the normalized attenuation constant, in which we can see the relationship among the three variables. FOM remains almost stable in the range $0.55 \leqslant h/w \leqslant 0.7$, and it achieves the maximum value at the point of $h/w=0.618$.

3.7 Coupling length

In addition to the basic characteristics of the waveguide in the preceding research, there is crosstalk between two adjacent waveguides in actual process. Therefore, in order to integrate the photon components into a chip, the coupling length between the adjacent waveguides needs taking into consideration. This is due to the fact that the coupling efficiency between the two waveguides depends on the spatial field distribution rather than the mode width. Therefore, the calculation of the coupling length is defined by the mode effective index difference between the symmetric and the asymmetric modes[25],

$$L_{\mathrm{coupl}}=\frac{\lambda_0}{2\times(N_+-N_-)}, \tag{4}$$

where N_+ and N_- are the mode effective refractive indexes of the symmetric and the asymmetric modes, respectively. The coupling length calculation includes two cases, which are waveguide′s horizontal placement and vertical placement, respectively. Because a substrate structure with double layers of silicon and silica is used, the waveguide is asymmetric in the vertical direction. Hence, the coupling length calculation of the proposed waveguide uses the waveguide′s horizontal placement[18]. The curve of the coupling length versus the separation distance S between two adjacent waveguides is shown in Fig. 8. The calculated results indicate that when the distance of the two adjacent waveguides is more than 3 μm, the coupling length is over 5 times of the propagation distance. The crosstalk can be ignored when the coupling length is larger than 5 times of the propagation distance[24]. Consequently, the proposed waveguides have a much better isolation distance.

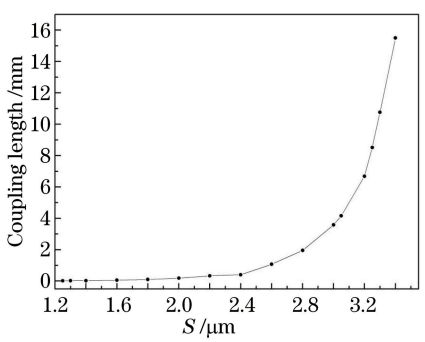

Fig. 8 Curves of the coupling length of two adjacent waveguides versus the center-to-center separation distance S

4 Conclusion

A novel LR-DLSPPW based on the golden ratio is proposed, and the numerical simulations are conducted at the telecom wavelength $\lambda_0=1.55$ μm by using the FEM. The results indicate that this structure does not only confine the mode field in the golden rectangle ridge, but also has better transmission characteristics. When the dielectric ridge is the golden rectangle, meaning that the height-width ratio of the dielectric ridge is the golden ratio, and when the dielectric ridge area is 0.9 μm^2, this waveguide has a relatively longer propagation distance $L_p=1.36$ mm and a relatively smaller mode width of 1.35 μm. In this situation, the waveguide also has a maximum value for FOM that exceeds 6.15×10^5. Due to the fact that FOM is a key factor to estimate the overall waveguide performance, this kind of waveguide has better transmission characteristics when compared with the dielectric ridge of other shapes. Finally, the coupling length of the two adjacent waveguides is also calculated and it indicates that the crosstalk between the two waveguides can be avoided when the distance of the two adjacent waveguides is larger than 3 μm. Consequently, the proposed LR-DLSPPW based on the golden ratio does not only have relatively better transmission characteristics, but also has significant potential for application to the design of the plasmonic waveguide components and high density integrated optoelectronic circuits.

Reference

1 Krasavin A V, Zayats A V. Guiding light at the nanoscale: Numerical optimization of ultrasubwavelength metallic wire

plasmonic waveguides[J]. Optics Letters, 2011, 36(16): 3127-3129.
2 Barnes W L, Dereux A, Ebbesen T W. Surface plasmon subwavelength optics[J]. Nature, 2003, 424(6950): 824-830.
3 Chiu N F, Lin C W, Lee J H, *et al*.. Enhanced luminescence of organic/metal nanostructure for grating coupler active long-range surface plasmonic device[J]. Applied Physics Letters, 2007, 91(8):083114.
4 Zhao Hai, Song Qing, Sun Haili, *et al*.. Study on transmission characteristics of a hybrid triangle wedge surface plasmonic polaritons waveguide with subwavelength mode confinement[J]. Laser & Optoelectronics Progress, 2015, 52(9): 091301.
赵 海, 宋 卿, 孙海丽,等. 一种具有亚波长模式限制的三角楔形混合表面等离子激元波导传输特性研究[J]. 激光与光电子学进展, 2015, 52(9): 091301.
5 Verhagen E, Spasenovic M, Polman A, *et al*.. Nanowire plasmon excitation by adiabatic mode transformation[J]. Physical Review Letters, 2009, 102(20): 203904.
6 Pyayt A L, Wiley B, Xia Y, *et al*.. Integration of photonic and silver nanowire plasmonic waveguides[J]. Nature Nanotechnoly, 2008, 3(11): 660-665.
7 Bozhevolnyi S I, Volkov V S, Devaux E, *et al*.. Channel plasmon subwavelength waveguide components including interferometers and ring resonators[J]. Nature, 2006, 440(7083): 508-511.
8 Holmgaard T, Bozhevolnyi S I. Theoretical analysis of dielectric-loaded surface plasmon polariton waveguides[J]. Physical Review B, 2007, 75(24): 245405.
9 Krasavin A V, Zayats A V. Passive photonic elements based on dilectric-loaded surface plasmon polariton waveguides[J]. Applied Physics Letters, 2007, 90(21): 211101.
10 Holmgaard T, Bozhevolnyi S I, Markey L, *et al*.. Dielectric-loaded surface plasmon-polariton waveguides at telecommunication wavelengths: Excitation and characterization[J]. Applied Physics Letters, 2008, 92(1): 011124.
11 Zhang Guanmao, Sun Haili, Li Jianming, *et al*.. Study on the transmission characteristics of symmetric hybrid long-range surface plasmon polariton waveguide[J]. Laser & Optoelectronics Progress, 2013, 50(12): 121301.
张冠茂, 孙海丽, 李建明,等. 一种对称混合长程表面等离子激元波导传输特性研究[J]. 激光与光电子学进展, 2013, 50(12):121301.
12 Burke J J, Stegeman G I, Tamir T. Surface-polariton-like waves guided by thin, lossy metal films[J]. Physical Review B, 1986, 33(8):5186-5201.
13 Charbonneau R, Bernin P, Berolo E, *et al*.. Expermental observation of plasmon-polariton waves supported by a thin metal films of finite width[J]. Optical Letters, 2000, 25(11):844-846.
14 Wang Jicheng, Liu Hongjiao, Cai Zengyan, *et al*.. Design of surface plasmon dichroic splitter with two metallic slits[J]. Laser & Optoelectronics Progress, 2014, 51(10): 102301.
王继成, 刘红娇, 蔡增艳, 等. 双缝波导结构表面等离子体可见光分束器设计[J]. 激光与光电子学进展, 2014, 51(10): 102301.
15 Shi Zhendong, Zhao Haifa, Liu Jianlong, *et al*.. Design of a metallic waveguide all-optical switch based on surface plasmon polaritons[J]. Acta Optica Sinica, 2015, 35(2): 0213001.
石振东, 赵海发, 刘建龙, 等. 基于表面等离激元的金属波导全光开关设计[J]. 光学学报, 2015, 35(2): 0213001.
16 Wang Jicheng, Jiang Yalan, Wang Yueke, *et al*.. Directional couplers based on MIM plasmonic waveguide stuctures[J]. Chinese J Lasers, 2015, 42(2): 0217001.
王继成, 蒋亚兰, 王跃科, 等. 基于 MIM 结构等离子体波导定向耦合器[J]. 中国激光, 2015, 42(2): 0217001.
17 Wang Zhibin, Han Huanhuan. Study of prism surface plasmons resonances senor based on double dielectric layers[J]. Acta Photonica Sinica, 2015, 44(10): 1024001.
王志斌, 韩欢欢. 基于双电介质层的棱镜表面等离子共振传感的研究[J]. 光子学报, 2015, 44(10): 1024001.
18 Gosciniak J, Holmgaard T, Bozhevolnyi S I. Theoretical analysis of long-range dielectric-loaded surface plasmon polariton waveguides[J]. Journal of Lightwave Technology, 2011, 29(10): 1473-1481.
19 Berini P. Figures of merit for surface plasmon waveguides[J]. Optics Express, 2006, 14(26): 13030-13042.
20 Krasavin A V, Zayats A V. Numerical analysis of long-range surface plasmon polariton modes in nanoscale plasmonic waveguides[J]. Optics Letters, 2010, 35(13) : 2118-2120.
21 O′Connor D, McCurry M, Lafferty B, *et al*.. Plasmonic waveguide as an efficient transducer for high-density data storage [J]. Applied Physics Letters, 2009, 95(17): 171112.
22 Krasavin A V, Zayats A V. All-optical active components for dielectric-load plasmonic waveguides[J]. Optics Communications, 2010, 283(8): 1581-1584.
23 Volkov V S, Han Z H, Nielsen M G, *et al*.. Long-range dielectric-load surface plasmon polariton waveguides operating at telecommunication wavelengths[J]. Optics Letters, 2011, 36(21): 4278-4280.
24 Krasavin A V, Zayats A V. Silicon-based plasmonic waveguides[J]. Optics Express, 2010, 18(11): 11791-11799.
25 Shi X L, Zhang X M, Han Z H, *et al*.. CMOS-compatible long-range dielectric-load plasmonic waveguides[J]. Journal of Lightwave Technology, 2013, 31(21): 3361-3367.

26 Rao R, Tang T. Study on active surface plasmon waveguides and design of a nanoscale lossless surface plasmon waveguide [J]. Journal of the Optical Society of America B, 2011, 28(5): 1258-1265.

27 Palik E D. Handbook of optical constants of solids[M]. Boston: Academic Press, 1985.

28 Li Y E, Zhao H, Ma A N, *et al*.. Semi-elliptical dielectric-loaded surface plasmon-polariton waveguides[J]. Optics Communications, 2011, 284(12): 2839-2842.

29 Han Z H, Bozhevolnyi S I. Radiation guiding with suface plasmon polaritons[J]. Reports on Progress in Physics, 2013, 76(1): 16402-16438.